Finite element modeling and bending analysis of piezoelectric sandwich beam with debonded actuators

K. Venkata Rao[1], S. Raja[*2] and T. Munikenche Gowda[3]

[1]*Department of Mechanical Engineering, B.M.S Evening College of Engg., Bangalore- 560019, India*
[2]*Structural Technologies Division, CSIR-National Aerospace Laboratories, Bangalore-560017, India*
[3]*Principal, S.J.C. institute of Technology, Chickballapur-562101, India*

Abstract. The present work pays emphasis on investigating the effect of different types of debonding on the bending behaviour of active sandwich beam, consisting of both extension and shear actuators. An active sandwich beam finite element is formulated by using Timoshenko's beam theory, characterized by first order shear deformation for the core and Euler-Bernoulli's beam theory for the top and bottom faces. The problem of debondings of extension actuator and face are dealt with by employing four-region model for inner debonding and three-region model for the edge debonding respectively. Displacement based continuity conditions are enforced at the interfaces of different regions using penalty method. Firstly, piezoelectric actuation of healthy sandwich beam is assessed through deflection analysis. Then the effect of actuators' debondings with different boundary conditions on bending behavior is computationally evaluated and experimentally clamped-free case is validated. The results generated will be useful to address the damage tolerant design procedures for smart sandwich beam structures with structural control and health monitoring applications.

Keywords: sandwich beam; piezoelectric actuator; extension actuation mechanism (EAM); shear actuation mechanism (SAM); hybrid actuation mechanism (HAM); debonding

1. Introduction

Piezoelectric actuator/sensor based smart structures have been evolved as the most promising and reliable structural elements for on-board static shape and dynamic control to achieve improved performances in the field of aerospace structural systems. Piezoelectric structures offer the advantages of quick dynamic response, low power consumption, low cost etc. Research works on beams with piezoelectric actuators had addressed various modeling issues with static and dynamic control applications (Li *et al.* 2003, Kusculuoglu *et al.* 2004, Wang 2004, Lee 2005, Kumar *et al.* 2008, Kapuria and Yaqoob Yasin 2010, Singh *et al.* 2011). A recent review by Kapuria *et al.* (2010) on piezoelectric composite laminates presented the state-of-the-art and future challenges, focusing on the need of efficient analysis models and their numerical implementation with particular emphasis on dynamic control, micromechanical behavior of material etc.

∗Corresponding author, Senior Principal Scientist, E-mail: raja@nal.res.in

Perfect bonding of actuators and sensors in a piezoelectrically actuated structural member is crucial for effective strain transfer from actuator to the host structure and from the host structure to the sensor. Improper bonding or debonding of active elements leads to significant drop in the actuation performance, sensor faultiness etc., if not the complete failure of the actuation process in the smart structures. Few research works reported in this field are related to the development of analytical and numerical models and the study of closed loop vibration control, mode shapes etc. Seeley and Chattopadyay (1998) investigated the effect of edge debonded actuator on the mode shapes and frequencies. Finite element formulation based on refined third order theory was developed. It was found that increase in debonded length of actuator introduces global and local deformations leading to significant changes in mode shapes and frequencies. Sun and Tong (2004) developed an eigen value problem for a composite beam with debonded actuators to study the effect of edge debonded actuators on the open loop and closed loop behavior.

Nagendra Kumar *et al*. (2007) investigated the effect of debonding of multiple actuators from the host laminate on the performance of the closed loop vibration control. The control influence matrix was updated to represent the debonding in the distributed actuators. Sun *et al*. (2001) studied the influence of debonded actuator on the vibration control of active beam using classical beam theory. The model had included adhesive layer that allowed peel stresses and shear strain to be determined. Ikeda *et al*. (2010) carried out a linear finite element analysis on a beam with two symmetrically inner debonded top and bottom actuators. It was shown that the inner debonded actuator functions normally until it is buckled. Furthermore, the same was confirmed by using a non-linear finite element analysis.

The concept of piezoelectric sandwich beam incorporating both extension and shear actuators was developed for the sole purpose of augmenting actuation authority. Hybrid actuation mechanism (HAM), in a sandwich beam employs both extension actuation mechanism (EAM) and shear actuation mechanism (SAM) to function simultaneously. Several numerical and analytical investigations were carried out to address the issues of modelling and analysis of piezoelectric sandwich beams regarding the actuation authority, vibration control etc. A unified finite element formulation of adaptive sandwich beam, capable of modeling either extension or shear actuation mechanism was presented by Benjeddou *et al*. (1997). It was shown that the shear actuation mechanism is better suited for stiff structures with thick piezoelectric actuators than the extension actuation mechanism. Raja *et al*. (2002) developed a coupled finite element procedure using a two node beam element, which is able to simulate both extension and shear actuations. Modal control studies were performed on the sandwich-laminated beams. Kapuria and Alam (2006) presented an efficient finite element model based on layerwise (zigzag) theory for the dynamic analysis of smart composite and sandwich beams. The other important research works reported on the analytical and numerical models for the static and dynamic analyses of active sandwich beam include, Aldraihem *et al*. (2000), Khadeir *et al*. (2001), and Baillargeon and Vel (2005), Manjunath and Bandyopadhyay (2009).

HAM may find application in the fields of vibration control, energy harvesting, and structural health monitoring due to augmented actuation authority. In this direction, a unified coupled layerwise theory was presented by Kapuria and Hagedorn (2007) for modelling the hybrid actuated laminated beams with extension and shear piezoelectric actuators and sensors. Constitutive equations for plane stress and plane strain beams with arbitrary poling direction were derived using transformation rules. The theory considered a third-order variation across the thickness with a layerwise linear variation for the axial displacement and a piecewise quadratic electric potential distribution across the sublayers. Further a beam element was derived with two physical nodes for

mechanical degrees of freedom and an electric node to represent the electric potentials of electrode surfaces of active patches, which reduces the number of electric degrees of freedom substantially. An important outcome of the study was that the ability of an actuator in inducing deflection for a given energy increases with thickness for both extension and shear mode actuations.

1.1 Significance and outline of the present work

As the piezoelectric adaptive sandwich beam, employing both extension and shear actuators contains many bonded surfaces, there is greater probability of occurrence of debonding due to impact and other operational loadings. Debonding in a crucial layer (for example face debonding), seriously affects the actuation authority of both extension and shear actuators. Study of behaviour of adaptive sandwich beam in the presence of debonded actuators assumes significance due to the following facts.

- Bending deflection behaviour of an active beam with a debonded layer is dependent on diverse factors namely, length of debonding, type of debonding (edge/inner debonding), location of debonded layer, boundary conditions, type of actuation (EAM/SAM/HAM) etc. Therefore, precise understanding of the bending behaviour of an adaptive sandwich beam under these conditions is very important for the implementation of corrective measures in a closed loop control system.
- Standard finite element software such as ANSYS, ABAQUS etc., provides elements with electromechanical coupling capability. Nevertheless, these elements incorporating only C^0 continuous interpolation functions, which may result in requirement of large number of elements for modeling piezoelectric actuators under bending. In case of a solid element such as SOLID5 in ANSYS which does support layered construction, aspect ratio becomes an issue, when the thickness of the actuator layer is very thin (in microns), thus requiring very large number of elements. Therefore, a simplified beam model employing Hermitian shape functions would be beneficial to quickly analyze bending and shear actuations. The present finite element procedure yields the results with few elements (20 beam elements) which are closer to those obtained from analytical solution. On the other hand, in ANSYS more than 10,000 solid elements had to be used to model debonding in a sandwich beam.

Thus bending behaviour of sandwich beam is studied by considering, 1.debonding of extension actuator from the top face and 2.debonding of top face from shear actuator. Two different types of debonding considered for the study include edge debonding and inner debonding. The reason for considering debonding of face consisting of both elastic substrate and surface bonded actuator is that it leads to severe loss of bending stiffness, in addition to reduction in effective length of the actuator. The present work involves 1.Formulation of two noded piezoelectric sandwich beam element with the capabilities of extension actuation, shear actuation and hybrid actuation mechanisms, 2.Development of displacement continuity conditions between different regions of debonded beam and experimental validation of extension actuator debonding, 3. Implementation of displacement continuity conditions using a systematic procedure and 4. Investigation on deflection behaviour of sandwich beam with different types of debonding (edge debonding and inner debonding), actuation types (extension, shear and hybrid actuations) and boundary conditions. The implementation is done using MATLAB software.

2. Kinematic relations for the active sandwich beam

Deflection of the sandwich beam on x-z coordinate system (Fig. 1(a)), under the influence of electrical/mechanical loads may be expressed in terms of displacements at the reference axis; in-plane displacement u_0 along x-axis, rotation θ_y due to transverse shear deformation in the x-z plane, transverse deflection w_0 and slope $w_{0,x}$. The details of deformation are pictured in Fig. 1(b). Transverse plane *abcd* before deformation becomes *a'b'c'd'* after deformation. The rotation θ_y is the angle between normal to x-axis before deflection and the line joining the midpoints of the top and bottom faces after deflection. The strain vector related to the reference plane displacements are

$$\{\varepsilon\} = \begin{bmatrix} \varepsilon_c^m & \varepsilon_c^{gb} & \varepsilon_i^{lb} & \gamma_{xz}^s \end{bmatrix}^T \tag{1}$$

where, ε_c^m is the in-plane strain at the reference axis, $\varepsilon_c^{gb}(=\theta_{y,x})$ is the global curvature due to shear deformation, $\varepsilon_i^{lb}(=w_{0,xx})$ is the curvature due to transverse deflection w_0 and γ_{xz}^s is the transverse shear strain in the sandwich, which is the angle between the line through the mid-surfaces of the two faces and normal to the deformed reference surface. Shear strain γ_{xz}^c in the core is defined as the angle between a line normal to the undeformed core and normal to the deformed reference surface. With the knowledge of displacements and strains at the reference axis of the sandwich, the displacements and strains at the axes and arbitrary points (*p*) in the top and bottom faces and core may be determined.


(a)   (b)
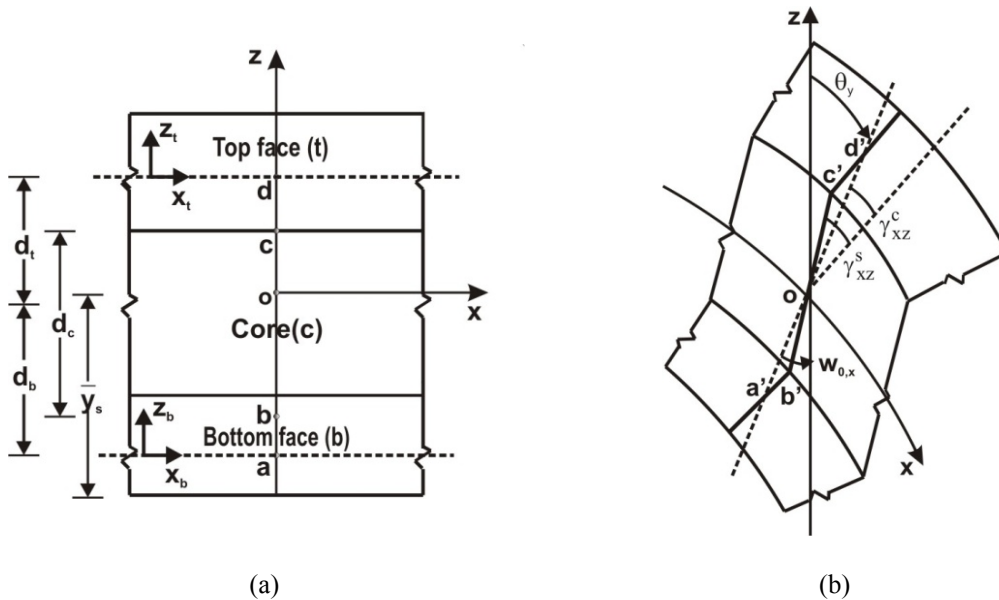
Fig. 1 Sandwich beam (a) before deformation and (b) after deformation

Displacements

$$u_c^m (x,z,t) = u_0 (x,t)$$
$$u_c^p (x,z,t) = u_0 (x,t) + z\theta_y (x,t)$$
$$w(x,z,t) = w_0 (x,t) \tag{2}$$

$$u_i^m (x,z,t) = u_0 (x,t) \pm d_i \theta_y (x,t), \ i=(+)t, (-)b$$
$$u_i^p (x,z,t) = u_0 (x,t) \pm d_i \theta_y (x,t) - (z-d_i) w_{o,x} (x,t)$$
$$w(x,z,t) = w_0 (x,t) \tag{3}$$

Strain components

$$\varepsilon_c^m = u_{o,x}$$
$$\varepsilon_c^b = \theta_{y,x}$$
$$\varepsilon_c^p = u_{o,x} + z\theta_{y,x}$$
$$\gamma_{xz}^c = \theta_y + \frac{\partial w_o}{\partial x} \tag{4}$$

$$\varepsilon_i^m = u_{o,x} \pm d_i \theta_{y,x}, \ i=(+)t, (-)b$$
$$\varepsilon_i^p = \varepsilon_{xi}^m - (z-d_i) w_{o,xx}$$
$$\varepsilon_i^b = -w_{o,xx} \tag{5}$$

where the superscripts are m: membrane, *b*: bending, *p*: arbitrary point, *s*: transverse shear, the subscripts are *c*: core, i = top face (*t*) and bottom face (*b*), and z is the distance of an arbitrary point *p*.

3. Coupled constitutive equations

Transverse linear electric potential in the extension and shear actuators is

$$\varphi_i = \frac{(z^{(i)} - h_{k-1}^{(i)})}{(h_k^{(i)} - h_{k-1}^{(i)})} \varphi_{1i} \tag{6}$$

where, $\varphi_{1i} = \varphi_i^+ - \varphi_i^-$, $i = t, b, c$; in which φ_{1i} is the difference of potential, φ_i^+ is the applied potential on the top electrode, φ_i^- is the potential in the bottom electrode, and h_k and h_{k-1} are the distances of the surfaces of the kth layer from the mid-plane of the sub-laminate (core/or face). The transverse electric field component in the extension/shear actuator is given by,

$$E_{3i} = -\frac{1}{(h_k^{(i)} - h_{k-1}^{(i)})} \varphi_{1i}, \quad i = t, b, c \tag{7}$$

The constitutive equations are derived by considering the fact that the piezoelectric material is elastically orthotropic and piezoelectrically orthorhombic of class mm2. Kapuria and Hagedorn (2007) presented unified constitutive equations for both plane stress and plane strain beams by considering the arbitrary poling direction. In the present work, the axes of principal material

symmetry of the piezoelectric layers are taken to be aligned with axes of the sandwich beam.

For EAM, the applied electric field (E_3) parallel to the poling axis (along the thickness) of the extension actuators induces longitudinal strain. The constitutive equations for extension actuation (plane stress condition), involving elastic, piezoelectric and dielectric constants in the principal material coordinate system are given by

$$\begin{Bmatrix} \sigma_1 \\ D_3 \end{Bmatrix} = \begin{bmatrix} Q_{11}^* & -e_{31}^* \\ e_{31}^* & \eta_{33}^* \end{bmatrix} \begin{Bmatrix} \varepsilon_1 \\ E_3 \end{Bmatrix} \tag{8}$$

where $\qquad Q_{11}^* = C_{11} - \dfrac{C_{13}\,C_{13}}{C_{33}} \; ; \quad e_{31}^* = e_{31} - \dfrac{C_{13}\,e_{33}}{C_{33}} \; ; \quad \eta_{33}^* = \eta_{33} + \dfrac{e_{33}\,e_{33}}{C_{33}}$

From the preceding equation, it is clear that the extension actuation mechanism involves electromechanical coupling between the transverse electric field (E_3) and axial strain (ε_1). For shear actuation, the axially poled shear actuator in the core is subjected to the through-thickness electric field. The constitutive equations after the coordinate transformation (Kapuria and Hagedorn (2007) and Benjeddou *et al.* (1999)) are

$$\begin{Bmatrix} \sigma_1 \\ \sigma_5 \\ D_3 \end{Bmatrix} = \begin{bmatrix} Q_{33}^* & 0 & 0 \\ 0 & Q_{55}^* & -e_{15}^* \\ 0 & e_{15}^* & \eta_{11}^* \end{bmatrix} \begin{Bmatrix} \varepsilon_1 \\ \varepsilon_5 \\ E_3 \end{Bmatrix} \tag{9}$$

where $\qquad Q_{33}^* = C_{33} - \dfrac{C_{13}\,C_{13}}{C_{11}} \quad Q_{55}^* = C_{55} \; ; \quad e_{15}^* = e_{15} \; ; \quad \eta_{11}^* = \eta_{11}$

The presence of e_{15}^* in Eq. (10) leads to electromechanical coupling between transverse electrical field and shear strain.

4. Energy in piezoelectric sandwich beam

Electromechanical energy of internal forces as the sum of electromechanical energies in the top face, bottom face and core is

$$H = \sum_{i=t,\,b} H_i + H_c = -\frac{1}{2} \int_V \left(\sigma^{\mathrm{T}} \varepsilon - E^{\mathrm{T}} D \right) dV \tag{10}$$

By substituting the relations given by Eqs. (7)-(9) into Eq. (10) and integrating over the thicknesses, we get

$$H_i = \frac{1}{2} \sum_{j=1}^{2} \int_0^L \left(Q_{11_{ij}}^* \left(A_{ij}\varepsilon_i^m\varepsilon_i^m + 2I_{ij}^{bm}\varepsilon_i^m\varepsilon_i^b + I_{ij}^b\varepsilon_i^b\varepsilon_i^b \right) + 2e_{31_{ij}}^* \frac{\varphi_{1i}}{t_{ij}} \left(A_{ij}\varepsilon_i^m + I_{ij}^{bm}\varepsilon_i^b \right) \right.$$
$$\left. - \eta_{33_{ij}}^* A_{ij} \frac{\varphi_{1i}}{t_{ij}} \frac{\varphi_{1i}}{t_{ij}} \right) dx, \quad i=t,\,b$$

$$H_c = \frac{1}{2} \int_0^L \left[Q_{33_c}^* \left(A_c \varepsilon_c^m \varepsilon_c^m + 2I_c^{bm} \varepsilon_c^m \varepsilon_c^b + I_c^b \varepsilon_c^b \varepsilon_c^b \right) + Q_{55_c}^* A_c \varepsilon_c^S \varepsilon_c^S + 2e_{15_c}^* \frac{\varphi_{1c}}{t_c} \left(A_c \varepsilon_c^S \right) - \eta_{11_c}^* A_c \frac{\varphi_{1c}}{t_c} \frac{\varphi_{1c}}{t_c} \right] dx \qquad (11)$$

where, i is the index for the top face (t) and bottom face (b), j is the index for the two layers in each of the two faces, A is cross-sectional area, I^{bm} is first moment of area and I^b is second moment of area.

Virtual work done by external mechanical forces is derived by considering that the layers in the top and bottom faces and the core are subjected to the traction (T) along x and z directions.

$$W_i = \left(t_i^x u_i^m - m_i^S w_{0,x} + t_i^z w_0 \right)\Big|_0^L, \quad i = t, b$$

$$W_c = \left(t_c^x u_0 + m_c^S \theta_y + t_c^z w_0 \right)\Big|_0^L \qquad (12)$$

Net forces in the top/bottom faces (t_i^x and t_i^z) and core (t_c^x and t_c^z) are obtained by integrating the traction forces (T_{ij}^x and T_{ij}^z) in the top/bottom face and those (T_c^x and T_c^z) in the core over the thicknesses. Similarly the net moments due to traction force in the top/bottom faces (m_i^S and m_i^B) and those in the core (m_c^S and m_c^B) are estimated by integrating the product of traction/body force and the moment arm over the areas.

5. Finite element formulation of piezoelectric sandwich beam element

Two noded piezoelectric sandwich beam element is developed with four mechanical degrees of freedom and three electrical degrees of freedom per node. Bottom electrodes of extension actuators and shear actuator are assumed to be grounded. Therefore the potential is applied on the top electrode only. Thus the difference of electrical potentials will be the electrical degrees of freedom. The nodal degrees of freedom for the element are,

$$\{u^e\} = \left[\tilde{u}_{0_1}^e \; \tilde{\theta}_{y_1}^e \; \tilde{w}_{0_1}^e \; \tilde{w}_{0,x_1}^e \; \tilde{\varphi}_{1t_1}^e \; \tilde{\varphi}_{1b_1}^e \; \tilde{\varphi}_{1c_1}^e \; \tilde{u}_{0_2}^e \; \tilde{\theta}_{y_2}^e \; \tilde{w}_{0_2}^e \; \tilde{w}_{0,x_2}^e \; \tilde{\varphi}_{1t_2}^e \; \tilde{\varphi}_{1b_2}^e \; \tilde{\varphi}_{1c_2}^e \right]^T \qquad (13)$$

C^0 interpolated linear Lagrange shape functions are used for the displacements $\tilde{u}_0^e$, $\tilde{\theta}_y^e$ and electric potentials φ_{1i} (Raja *et al.* 2002), and C^1 interpolated cubic Hermite shape functions are used for w_0, as Euler-Bernoulli beam theory is adopted for top and bottom faces. The strain-displacement and electric field-potential relations in global coordinates are,

$$\{\varepsilon_i^m\} = \sum_{k=1}^2 [J]^{-1} \left[B_m^{(i)} \right]_k col(\tilde{u}_0^e \; \tilde{\theta}_y^e)_k$$

$$\{\varepsilon_i^b\} = \sum_{k=1}^2 [J]^{-1} \left[B_b^{(i)} \right]_k col(\tilde{w}_0^e \; \tilde{w}_{0,x}^e)_k, \quad i = t, b$$

$$\{\varepsilon_c^m\} = \sum_{k=1}^2 [J]^{-1} \left[B_m^{(c)} \right]_k col(\tilde{u}_0^e)_k$$

$$\{\varepsilon_c^b\} = \sum_{k=1}^2 [J]^{-1} \left[B_b^{(c)} \right]_k col(\tilde{\theta}_y^e)_k$$

$$\left\{\varepsilon_c^S\right\} = \sum_{k=1}^{2} [J]^{-1} \left[B_s^{(c)}\right]_k col\,(\widetilde{\theta}_y^e \ \ \widetilde{w}_0^e \ \ \widetilde{w}_{0,x}^e\,)_k$$

$$\left\{E_3^{(i)}\right\} = \sum_{k=1}^{2} [J]^{-1} \left[B_\varphi^{(i)}\right]\left\{\widetilde{\phi}_{1i}^e\right\}_k, \ i = t,\, b \ \text{and} \ c \tag{14}$$

where J is a Jacobian matrix, relating the local coordinate ξ and global x. $\mathbf{B}_m, \mathbf{B}_b, \mathbf{B}_s$ and $\mathbf{B}_\phi$ are elastic and electric gradient matrices. Column vector is denoted by 'col'. The elemental stiffness may be estimated by considering the discretized virtual work of electromechanical internal forces and applied mechanical forces as follows. The discretized virtual work of electromechanical internal forces in the top/bottom faces is

$$\delta\mathbf{H}_i^e = \delta\!\left(\widetilde{\mathbf{u}}^e\right)^T \left(\hat{\mathbf{K}}_{uu}^{(i)} + \hat{\mathbf{K}}_{u\phi}^{(i)} + \hat{\mathbf{K}}_{\phi u}^{(i)} + \hat{\mathbf{K}}_{\phi\phi}^{(i)}\right)\widetilde{\mathbf{u}}^e, \ i = t,\, b \tag{15}$$

$$\hat{\mathbf{K}}_{uu}^{(i)} = \sum_{j=1}^{2} \hat{\mathbf{K}}_{uu}^{(ij)}, \ \hat{\mathbf{K}}_{u\phi}^{(i)} = \sum_{j=1}^{2} \hat{\mathbf{K}}_{u\phi}^{(ij)}, \ \ \hat{\mathbf{K}}_{\phi u} = \hat{\mathbf{K}}_{u\phi}^{T}, \ \text{where} \ i = t,\, b$$

$$\hat{\mathbf{K}}_{uu}^{(ij)} = \int \left[Q_{11_{ij}}^* \left(A_{ij} \left(\mathbf{B}_m^{(i)}\right)^T \mathbf{B}_m^{(i)} + I_{ij}^{bm}\left(\left(\mathbf{B}_m^{(i)}\right)^T \mathbf{B}_b^{(i)} + \left(\mathbf{B}_b^{(i)}\right)^T \mathbf{B}_m^{(i)} \right) + I_{ij}^{b}\left(\mathbf{B}_b^{(i)}\right)^T \mathbf{B}_b^{(i)} \right) \right] \det\mathbf{J}\,d\xi$$

$$\hat{\mathbf{K}}_{u\phi}^{(ij)} = -\int \left[e_{31_{ij}}^* \left(A_{ij}\left(\mathbf{B}_m^{(i)}\right)^T + I_{ij}^{bm}\left(\mathbf{B}_b^{(i)}\right)^T \right)\mathbf{N}_\phi^{(ij)} \right] \det\mathbf{J}\,d\xi,$$

$$\hat{\mathbf{K}}_{\phi\phi}^{(ij)} = -\int \eta_{33_{ij}}^* \frac{A_{ij}}{t_{ij}^2}\left(\mathbf{N}_\phi^{(ij)}\right)^T \mathbf{N}_\phi^{(ij)} \det\mathbf{J}\,d\xi, \ \text{where} \ i = t,\, b \ \text{and}\ j = 1,\, 2$$

The discretized virtual work of electromechanical internal forces in the core is

$$\delta\mathbf{H}_c^e = \delta\!\left(\widetilde{\mathbf{u}}^e\right)^T \left(\hat{\mathbf{K}}_{uu}^{(c)} + \hat{\mathbf{K}}_{u\phi}^{(c)} + \hat{\mathbf{K}}_{\phi u}^{(c)} + \hat{\mathbf{K}}_{\phi\phi}^{(c)}\right)\widetilde{\mathbf{u}}^e \tag{16}$$

where

$$\hat{\mathbf{K}}_{uu}^{(c)} = \int \left[Q_{33_c}^* \left(A_c \left(\mathbf{B}_m^{(c)}\right)^T \mathbf{B}_m^{(c)} + I_c^{bm}\left(\left(\mathbf{B}_m^{(c)}\right)^T \mathbf{B}_b^{(c)} + \left(\mathbf{B}_b^{(c)}\right)^T \mathbf{B}_m^{(c)} \right) + I_c^{b}\left(\mathbf{B}_b^{(c)}\right)^T \mathbf{B}_b^{(c)} \right) \right.$$
$$\left. + k_s k_c Q_{55_c}^* A_c \left(\mathbf{B}_S^{(c)}\right)^T \left(\mathbf{B}_S^{(c)}\right) \right] \det\mathbf{J}\,d\xi$$

Shear stiffness k_s for the sandwich beam is computed as (Koconis 1994)

$$[K_s]_{\text{sandwich}} = \frac{d_s}{t_c}[K_s]_{\text{core}} \ \ , \ \text{s: shear and}\ d_s = d_t + d_b$$

$$\hat{\mathbf{K}}_{u\phi}^{(c)} = -\int \left[e_{15_c}^* A_c \left(\mathbf{B}_S^{(c)}\right)^T \mathbf{N}_\phi^{(c)} \right] \ \det\mathbf{J}\,d\xi$$

$$\hat{\mathbf{K}}_{\phi\phi}^{(c)} = -\int \eta_{11_c}^* \frac{A_c}{t_c^2}\left(\mathbf{N}_\phi^{(c)}\right)^T \mathbf{N}_\phi^{(c)} \det\mathbf{J}\,d\xi$$

The discretized virtual work of applied mechanical forces is

$$\delta\mathbf{W}^e = \delta\!\left(\widetilde{\mathbf{u}}^e\right)^T \hat{\mathbf{f}}_m^e \tag{17}$$

$\hat{\mathbf{f}}_m^e$ is the consistent nodal force vector. Finally the coupled finite element equations in terms of displacements and potentials are derived as

$$\sum_{i=t,b,c} \left(\left[\hat{\mathbf{K}}_{uu}^{(i)} \right] \{ \widetilde{\mathbf{u}}^e \} + \left[\hat{\mathbf{K}}_{u\phi}^{(i)} \right] \{ \widetilde{\boldsymbol{\varphi}}_a^e \} - \left\{ \left(\hat{\mathbf{f}}_m^e \right)^{(i)} \right\} \right) = 0$$

$$\sum_{i=t,b,c} \left(\left[\hat{\mathbf{K}}_{\phi u}^{(i)} \right] \{ \widetilde{\mathbf{u}}^e \} - \left[\hat{\mathbf{K}}_{\phi\phi}^{(i)} \right] \{ \widetilde{\boldsymbol{\varphi}}_s^e \} \right) = 0 \tag{18}$$

The Eq. (18) may be rewritten as

$$\{ \widetilde{\mathbf{u}}^e \} = \sum_{i=t,b,c} \left(\left[\hat{\mathbf{K}}_{uu}^{(i)} \right]^{-1} \left\{ \left(\hat{\mathbf{f}}_m^e \right)^{(i)} \right\} - \left[\mathbf{K}_{uu}^{(i)} \right]^{-1} \left[\hat{\mathbf{K}}_{u\phi}^{(i)} \right] \{ \widetilde{\boldsymbol{\varphi}}_a^e \} \right)$$

$$\{ \widetilde{\boldsymbol{\varphi}}_s^e \} = \sum_{i=t,b,c} \left[\hat{\mathbf{K}}_{\phi\phi}^{(i)} \right]^{-1} \left(\left[\hat{\mathbf{K}}_{\phi u}^{(i)} \right] \{ \widetilde{\mathbf{u}}^e \} \right) \tag{19}$$

The nodal displacements of an element are estimated by imposing known electric potentials $\{ \widetilde{\boldsymbol{\varphi}}_a^e \}$ and are given by the expression for $\{ \widetilde{\mathbf{u}}^e \}$. Subsequently, the unknown sensory potentials $\{ \widetilde{\boldsymbol{\varphi}}_s^e \}$ may be obtained by using the calculated displacements in each element due to the applied mechanical force. However, in the present study the active layers are considered only as actuators to perform the static piezoelectric analysis.

6. Displacement continuity conditions for modeling debonding

To effectively capture the influence of actuator/ face debonding of a given length and location on the displacement distribution, the beam is basically divided into two regions. They are healthy (perfectly bonded) and debonded regions. The debonded region is in turn divided into two parallel regions, which are above and below the plane of debonding (POD[*]), referred to as top debonded region and bottom debonded region respectively. Healthy region, bottom debonded region and top debonded region are respectively denoted by region1, region2 and region3 in Fig. 2. Continuity of displacements between different regions is established by using the displacements at the reference axes of the end faces, forming the junctions of these regions. The distances, $\bar{y}_{f_1}$ and $\bar{y}_{f_2}$ of neutral axes of top/bottom face from the elastic layer end and actuator layer end respectively are

$$\bar{y}_{f_1} = \frac{E_e \, t_e^2 + E_{act} \, t_{act}^2 + 2 \, E_{act} \, t_{act} \, t_e}{2 \left(E_e \, t_e + E_{act} \, t_{act} \right)}$$

$$\bar{y}_{f_2} = t_f - \bar{y}_{f_1} \tag{20}$$

The suffixes '*e*' and '*act*' represent elastic layer and actuator respectively and *E* is young's modulus. The distances of neutral axes of the top and bottom faces from the axis of healthy region are denoted by d_t and d_b respectively. The following are the continuity conditions to be imposed for the top extension actuator and top face debonding.

(a) Top extension actuator debonding   (b) Top face debonding
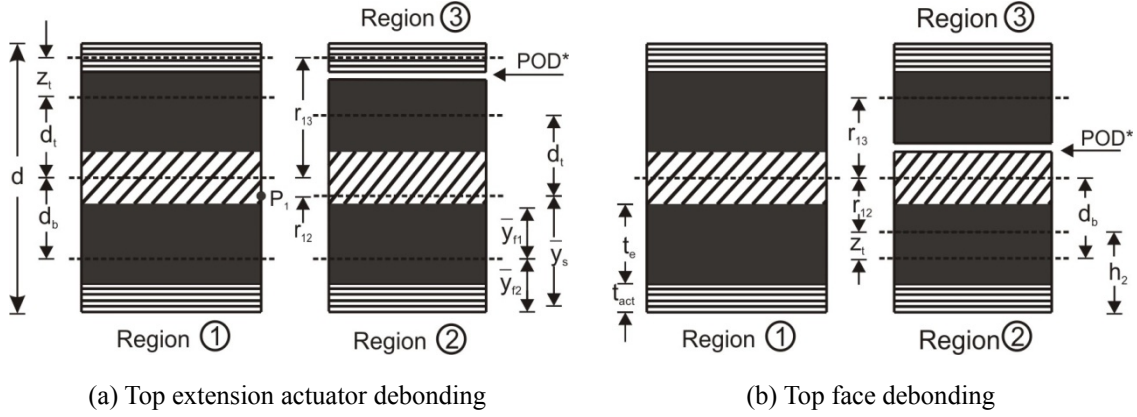
Fig. 2 Healthy and debonded regions

Case A: Top extension actuator debonding

Top debonded region (region3) consists of the top extension actuator, while the bottom debonded region (region2) has the layup scheme of (/top elastic layer (t_2) /core (*c*)/bottom elastic layer (b_2)/bottom extension actuator (b_1)/) as shown in Fig. (2(a)).

Healthy region-bottom debonded region: Both healthy region (region1) and bottom debonded region (region2) being sandwich beams, have the displacements u_0, θ_y, w_0 and $w_{0,x}$ at their reference axes. Hence the continuity of these displacements, at the interface between region1 and region2 has to be ensured. Distance between the axes of healthy region and bottom debonded region is

$$r_{12} = \frac{d}{2} - \bar{y}_s \tag{21}$$

where $\bar{y}_s$ is the location of the axis of bottom debonded region.

$$\mathrm{u}_{0_L}^{(2)} = \mathrm{u}_{0_R}^{(1)} - \mathrm{r}_{12}\,\theta_{y_R}^{(1)}$$
$$\theta_{y_L}^{(2)} = \theta_{y_R}^{(1)}\,;\,\mathrm{w}_{0_L}^{(2)} = \mathrm{w}_{0_R}^{(1)}\,;\,\mathrm{w}_{0,x_L}^{(2)} = \mathrm{w}_{0,x_R}^{(1)} \tag{22}$$

The notations are 1: region1, 2: region2, *R*: right side end of a region and *L*: left side end of a region. The axial displacement at point P_1 (Fig. 2(a)), on the right side end of the healthy region, and which is at a distance, r_{12} below the axis is equated to the displacement, $u_{0_L}^{(2)}$ of bottom debonded region at its left side end (Eq. (22)). The axial displacement at point P_1 is obtained from Eq. (2) for u_c^p, where the effect of rotation due to shear deformation is considered.

Healthy region-top debonded region: Euler-Bernoulli's beam theory is used for the top debonded region (region3), with the displacements, u_0, w_0 and $w_{0,x}$ at it's reference axis. Distance between the axes of top face and top extension actuator (z_t) and that between the axes of healthy region and top debonded region (r_{13}) are,

$$z_t = \frac{d}{2} - \left(d_t + \frac{t_{act}}{2} \right); \quad r_{13} = \frac{(d - t_{act})}{2} \tag{23}$$

Conditions for the continuity of displacements

$$u_{0_L}^{(3)} = u_{0_R}^{(1)} + \left(r_{13} - z_t \right) \theta_{y_R}^{(1)} - z_t \, w_{,x_R}^{(1)}$$

$$w_{0_L}^{(3)} = w_{0_R}^{(1)} \, ; w_{0,x_L}^{(3)} = w_{0,x_R}^{(1)} \tag{24}$$

where, t_t and t_b are thicknesses of top and bottom faces. Axial displacement $u_{0_L}^{(3)}$ of the top extension actuator in the healthy region is obtained by considering the effect of shear rotation and bending slope.

Case B: Top face debonding

Top debonded region (region3) consists of top face (/top extension actuator (t_1)/top elastic layer (t_2)/) and the bottom debonded region (region2) consists of core and bottom face (/core (c) /bottom elastic layer (b_2)/bottom extension actuator (b_1)/) as shown in Fig. 2(b).

Healthy region-bottom debonded region: Continuity of displacements, u_0, θ_y, w_0 and $w_{0,x}$ between healthy region (region1) and bottom debonded region (region2) is established through Eq. (26). In Eq. (25), h_2 is the location of the axis of the bottom debonded region and z_t is the distance between the axes of the bottom debonded region and bottom face.

$$h_2 = \frac{t_c + t_b}{2} \, ; r_{12} = \left(t_b + \frac{t_c}{2} \right) - h_2$$

$$z_t = d_b - r_{12} \tag{25}$$

$$u_{0_L}^{(2)} = u_{0_R}^{(1)} - \left(r_{12} + z_t \right) \theta_{y_R}^{(1)} - z_t \, w_{0,x_R}^{(1)}$$

$$\theta_{y_L}^{(2)} = \theta_{y_R}^{(1)} \, ; w_{0_L}^{(2)} = w_{0_R}^{(1)} \, ; w_{0,x_L}^{(2)} = w_{0,x_R}^{(1)} \tag{26}$$

Healthy region-Top debonded region: The top debonded region (region3) is treated as Euler-Bernoulli beam with the displacements, u_0, w_0 and $w_{0,x}$ at the reference axis. The displacement continuity conditions with respect to axial displacement, deflection and bending slope are

$$u_{0_L}^{(3)} = u_{0_R}^{(1)} + r_{13} \, \theta_{y_R}^{(1)}$$

$$w_{0_L}^{(3)} = w_{0_R}^{(1)} \, ; w_{0,x_L}^{(3)} = w_{0,x_R}^{(1)} \tag{27}$$

7. Implementation of continuity conditions

Finite element implementation of displacement continuity conditions demands that these

displacements be expressed in terms of the unknown nodal degrees of freedom. The discretization procedure results in different domains namely, healthy region, top debonded region and bottom debonded region, all attached to their respective axes. The interface between healthy region and bottom debonded region is represented by *S1* (r_1, r_2) and that between healthy region and top debonded region is represented by *S2* (r_1, r_3) as shown in Fig. 3. Here r_1, r_2 and r_3 represent healthy region, bottom debonded region and top debonded region respectively.

The procedure (Seeley and Chattopadyay 1999) outlined below is adopted for achieving symmetric set of equations for the application in the finite element model. The discretized conditions corresponding to the displacement continuity conditions given in Eqs. (22), (24), (26) and (27) in the matrix form are

$$\overline{\mathbf{R}}_1 \overline{\mathbf{u}}_1 = 0 \qquad (28)$$

where $\overline{\mathbf{R}}_1$ is the matrix consisting of coefficients of displacements in the displacement continuity equations, $\overline{\mathbf{u}}_1$ is the displacement vector corresponding to the nodes at the interfaces, l = S1, S2, S3 and S4 (Fig. 3) for inner debonding and l = S1 and S2 for edge debonding. Displacement vectors at the interfaces are

$$\overline{\mathbf{u}}^{\mathbf{S1}} = [\,\overline{\mathbf{u}}_R^{(1)}\ \overline{\mathbf{u}}_L^{(2)}\,]^T ; \quad \overline{\mathbf{u}}^{\mathbf{S2}} = [\,\overline{\mathbf{u}}_R^{(1)}\ \overline{\mathbf{u}}_L^{(3)}\,]^T$$

$$\overline{\mathbf{u}}^{\mathbf{S3}} = [\,\overline{\mathbf{u}}_R^{(2)}\ \overline{\mathbf{u}}_L^{(4)}\,]^T ; \overline{\mathbf{u}}^{\mathbf{S4}} = [\,\overline{\mathbf{u}}_R^{(3)}\ \overline{\mathbf{u}}_L^{(4)}\,]^T \qquad (29)$$

The interfacial displacement vectors related to healthy region, bottom debonded region and top debonded region for the edge debonding are

$$\left\{ \overline{\mathbf{u}}_R^{(1)} \right\} = \left[\widetilde{\mathbf{u}}_{0_R}^{(1)}\ \ \widetilde{\theta}_{y_R}^{(1)}\ \ \widetilde{\mathbf{w}}_{0_R}^{(1)}\ \ \widetilde{\mathbf{w}}_{0,x_R}^{(1)} \right]^T$$

$$\left\{ \overline{\mathbf{u}}_L^{(2)} \right\} = \left[\widetilde{\mathbf{u}}_{0_L}^{(2)}\ \ \widetilde{\theta}_{y_L}^{(2)}\ \ \widetilde{\mathbf{w}}_{0_L}^{(2)}\ \ \widetilde{\mathbf{w}}_{0,x_L}^{(2)} \right]^T$$

$$\left\{ \overline{\mathbf{u}}_L^{(3)} \right\} = \left[\widetilde{\mathbf{u}}_{0_L}^{(3)}\ \ \widetilde{\mathbf{w}}_{0_L}^{(3)}\ \ \widetilde{\mathbf{w}}_{0,x_L}^{(3)} \right]^T \qquad (30)$$

It is essential that in addition to satisfying the continuity of displacements, the continuity of velocities is also to be satisfied. This is achieved by differentiating Eq. (28) with respect to time *t*.

$$\overline{\mathbf{R}}_l \,\dot{\overline{\mathbf{u}}}_l = 0 \qquad (31)$$

The discretized total potential energy, including the penalty terms in the global coordinates is,

$$\Pi_{\mathbf{P}} = \left(\frac{1}{2}\, \dot{\widetilde{\mathbf{u}}}^T \mathbf{M} \dot{\widetilde{\mathbf{u}}} - \frac{1}{2} \widetilde{\mathbf{u}}^T \mathbf{K}\, \widetilde{\mathbf{u}} + \widetilde{\mathbf{u}}^T \widetilde{\mathbf{F}}_{\mathbf{m}} \right) + \left(\frac{1}{2} C_1\, \dot{\overline{\mathbf{u}}}^T \mathbf{R}^T \mathbf{R}\, \dot{\overline{\mathbf{u}}} - \frac{1}{2} C_2\, \overline{\mathbf{u}}^T \mathbf{R}^T \mathbf{R}\, \overline{\mathbf{u}} \right) \qquad (32)$$

The first, second and third terms correspond to kinetic energy, internal strain energy of elastic forces and potential energy of mechanical forces respectively. The fourth and fifth terms are the penalty terms related to the velocity and displacement continuity conditions respectively. The scalar constants C_1 and C_2 are chosen based on stiffness and mass matrices for use in the application of penalty method. The stationary value of the energy with respect to the degrees of freedom yields

$$\left[\mathbf{M} + C_1\,\mathbf{P}\right]\ddot{\widetilde{\mathbf{u}}} + \left[\mathbf{K} + C_2\,\overline{\mathbf{P}}\right]\widetilde{\mathbf{u}} - \widetilde{\mathbf{F}}_{\mathbf{m}} = \mathbf{0} \tag{33}$$

where, the mass and stiffness matrices are given by,

$$\mathbf{M} = \sum_n \mathbf{M}^{(n)} \text{ and } \mathbf{K} = \sum_n \mathbf{K}^{(n)}$$

where $n = r_1, r_2, r_3$ and r_4 for inner debonding and, $n = r_1, r_2$ and r_3 for edge debonding. The second healthy region in case of inner debonding is represented by r_4. $\mathbf{P}$ is the penalty matrix, which is used for imposing the continuity conditions and is computed as

$$\overline{\mathbf{P}}_1 = \overline{\mathbf{R}}_1^{\mathrm{T}}\,\overline{\mathbf{R}}_1 \tag{34}$$

Finally $\overline{\mathbf{P}}$ can be expressed in the form of

$$\overline{\mathbf{P}}_1 = \begin{bmatrix} \mathbf{P}_{ii} & \mathbf{P}_{ij} \\ \mathbf{P}_{ji} & \mathbf{P}_{jj} \end{bmatrix}_1 \tag{35}$$

where, $\mathbf{P}_{ji} = \mathbf{P}_{ij}^{T}$. The penalty matrix is expanded to the global degrees of freedom, so that it can be added to the global stiffness matrix. The penalty matrices for the top extension actuator debonding and top face debonding may be determined from Eq. (28) to Eq. (30) and Eq. (34) to Eq. (35). The penalty matrices are presented in Appendix A.
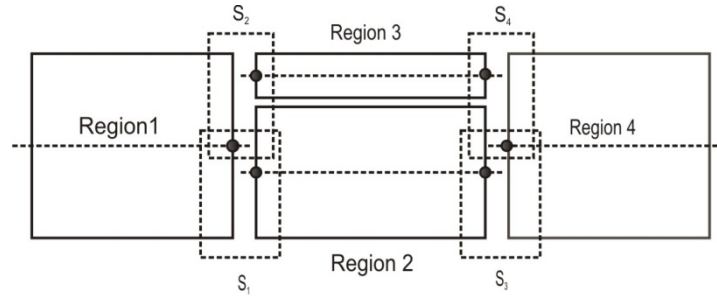
Fig. 3 Different regions in the inner debonded beam

8. Results and discussions

Dimensional details of the general form of sandwich beam with the segmented extension and shear actuators is shown in Fig. 4. Nevertheless, the study is carried out by considering the sandwich beam with full length extension and shear actuators (X_a = L/2 and L_a = L). Elastic substrates and the piezoelectric actuators are of aluminium and PZT-5H respectively. The properties of these materials are given in Table 1. The extension and shear actuators are subjected to $\pm 10V$ and $-20V$ respectively, in order to achieve extension, shear and hybrid actuations of the beam. Lengths of edge/inner debonded actuators are specified as a percentage of the length of the beam. The results obtained include deflection distributions under the influence of EAM, SAM

and HAM for the cases of healthy beam and the beam with different extents of edge debonding. Firstly, the following validations are carried out to verify the capabilities of the developed beam element and the debonding model.
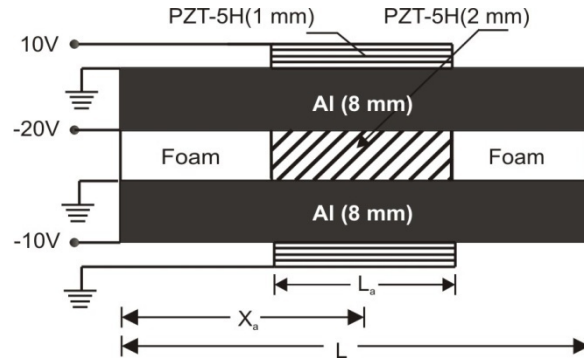
Fig. 4 Sandwich beam with segmented extension and shear actuators

Table 1 Material properties (Zhang 1996, Benjeddou 1999, Raja 2004)

- Aluminum:

$\rho = 2690.0 \text{Kg/m}^3$, $E = 70.3 \text{ GPa}$, $\nu = 0.343$

- PZT-5H:

$\rho = 7730.0 \text{ Kg/m}^3$

$$C = \begin{bmatrix} 126 & 79.5 & 84.1 & 0 & 0 & 0 \\ 79.5 & 126 & 84.1 & 0 & 0 & 0 \\ 84.1 & 84.1 & 126 & 0 & 0 & 0 \\ 0 & 0 & 0 & 23.3 & 0 & 0 \\ 0 & 0 & 0 & 0 & 23.3 & 0 \\ 0 & 0 & 0 & 0 & 0 & 23.3 \end{bmatrix} GPa$$

Piezoelectric coefficients: $d_{31} = -274.0$ m/V, $d_{15} = 741.0$ m/V, $d_{33} = 593.0$ m/V

Dielectric constants: $\eta_{11} = \eta_{22} = 1.508 \times 10^{-8}$ F/m, $\eta_{33} = 1.30 \times 10^{-8}$ F/m

- SP-5H[®] (www.sparklerceramics.com)

$\rho = 7500 \text{ Kg/m}^3$, $S_{11}^E = 21 \text{ m}^2 / \text{N}$, $S_{33}^E = 15 \text{ m}^2 / \text{N}$

Piezoelectric coefficients: $d_{31} = -265.0$ m/V, $d_{33} = 550.0$ m/V

Validation 1: Two separate active cantilever beams are considered for validation by verifying EAM and SAM actuation capability of the active sandwich beam element. The first consists of an

aluminum beam with surface bonded, full-length PZT-5H actuators and the second consists of a PZT-5H shear actuator, sandwiched between two aluminum substrates. The dimensional details of the beams are shown in Fig. 5. The first and second beams are subjected to EAM and SAM actuations respectively. Transverse displacement distributions of the beam are plotted as shown in Fig. 6(a), along with the results of Benjeddou *et al*. (1999) and those obtained from the analysis carried out by using ANSYS. The elements used for the ANSYS modeling are SOLID45 for the elastic substrates and SOLID5 with electromechanical coupling capability for piezoelectric actuators. The results of the present study match very well with those obtained by Benjeddou *et al*. (1999) and those from ANSYS modeling.

(a) Beam with extension actuators   (b) Beam with shear actuator
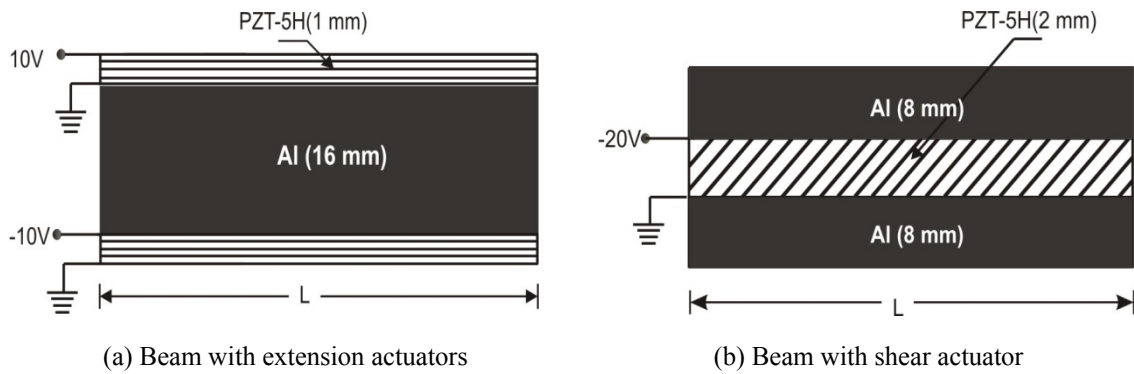
Fig. 5 Piezoelectric beams for validation

(a) Healthy beam under EAM and SAM   (b) Debonded beam under HAM
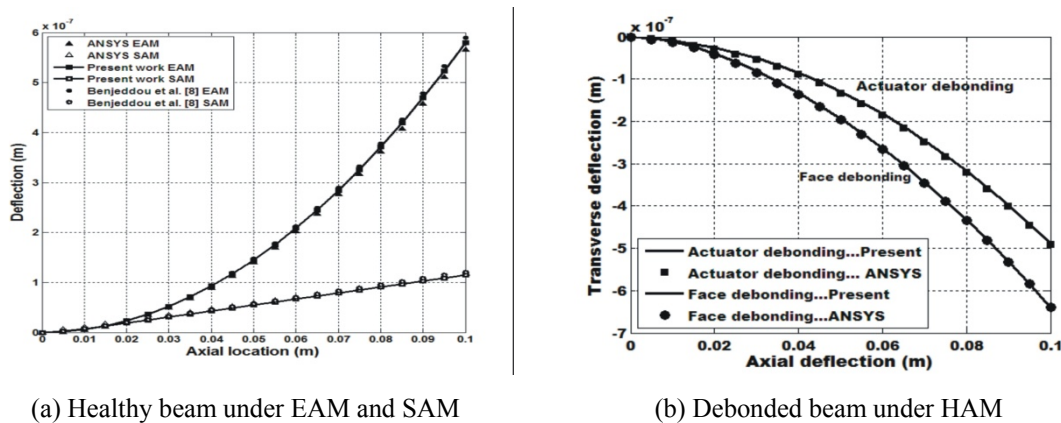
Fig. 6 Deflection distributions for validation

Validation 2: The authenticity of the model developed to represent the edge and inner debonding of extension actuator and face accurately is verified by using ANSYS. The sandwich beam with clamped-free boundary condition, used for modeling debonding has full-length

extension actuators and shear actuator. The extent and location of debonding considered are 20% edge debonding and on the fixed end side respectively. Deflection distributions obtained for the beam with i). Edge debonded top extension actuator under HAM and ii). Edge debonded top face under HAM and are plotted in Fig. 6(b) along with those obtained from ANSYS analysis. It is found that the results obtained from the present formulation are in agreement with those from the ANSYS analysis.

Validation 3: Experimental validation of edge debonding of extension actuator is carried out using two aluminium beam specimens of length 200mm and cross-sectional area (1.2 mm × 20 mm) with the top and bottom surface bonded SP-5H[®] (www.sparklerceramics.com, Sparkler, India) actuators of length 40 mm. Cross-sectional dimensions of the actuators is (0.5 mm×20 mm). The actuators are bonded right at the fixed end of the specimen. Actuators on the top surfaces of the two beams are edge debonded at the fixed end by a prescribed length (25% and 50% of the length of the actuator). Edge debonding is introduced in the actuators by using a very thin Teflon layer. Properties of aluminium and SP-5H[®] are given in Table 1. Deflection distributions are measured by using the experimental setup shown in Fig. (7). The instruments used are, 1.Oscilloscope, 2.Signal generator, 3.Multimeter, 4.Torque clamp, 5.Specimen, 6. Laser displacement sensor (20 μm sensitivity) and 7. High voltage amplifier (+/- 500 V). Top and bottom actuators are actuated individually by applying ±200 V. The deflections are measured along the length of the beam and the same are compared with the results obtained using the present debonding model. In the analysis, these experimental specimens are modeled with 20 elements. A very good correlation as shown in Fig. 8 is noticed between the analysis and the experiment, which shows the reliability of the proposed debonding model.
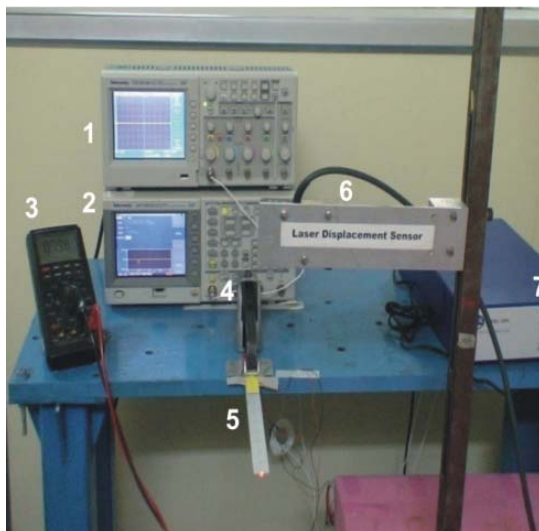
Fig. 7 Experimental setup   Fig. 8 Deflection distributions
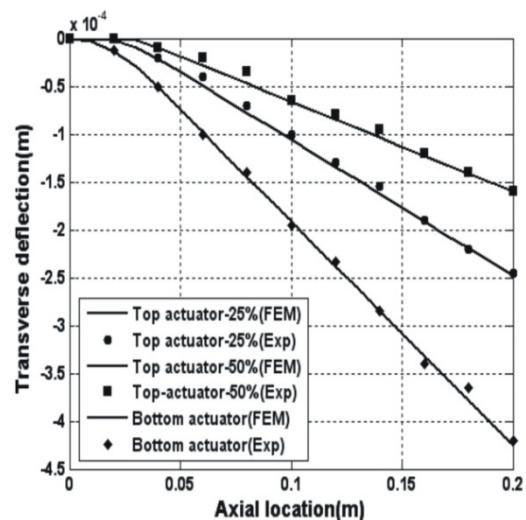
8.1 Debonding of top extension actuator

The extension actuator in the top/bottom face is a multifunctional layer, behaving as both elastic layer and actuator layer. Edge debonding of extension actuator results in altered bending stiffness and actuation authority; these in turn influence the electro-mechanical stiffness. This issue is addressed by carrying out several numerical experiments on two clamped-free beams and obtain, i) Deflection distributions of healthy beam with the entire lengths of top and bottom extension actuators being subjected to EAM (Fig. 9(a)). Also, the deflection distributions of healthy beam with the increasing length of dummy portion in the top extension actuator at the clamped end are obtained. The dummy portion in the top extension actuator is that portion which is not subjected to electrical potential. The lengths of dummy portion considered for the study are in the range of 10% and 50%, in steps of 10% of the actuator length. ii) Deflection distributions of the beam with edge debonded top extension actuator of different extents at the clamped end (Fig. 9(b)). The range of lengths of debonding is same as that of dummy portion in the healthy beam. Observe that the free end deflections of the healthy beam and debonded beam decrease with the increase in the length of the dummy portion of the extension actuator and increase in the length of debonded actuator respectively. However, for a given length of dummy portion in the extension actuator/debonded extension actuator, the deflection in the debonded beam is larger than that of healthy beam. Because, the healthy beam with a given length of dummy actuator is subjected to degradation in actuation authority, while its bending stiffness remains unaffected. On the other hand, the debonded beam is subjected to degradation in both bending stiffness and actuation authority.

Quantitatively, the free end deflection in the healthy beam with 30% dummy actuator portion is 0.3509 μm and that of beam with the same extent of debonding is 0.3527 μm. The difference between these values is equal to the additional deflection induced due to reduction in the bending stiffness of the beam. From this analysis, it is clear that the edge debonding of extension actuator leads to substantial degradation in actuation authority and negligible effect on bending stiffness. Next, the effect of SAM on the behavior of beam with debonded extension actuator is investigated.

Debonding of top extension actuator (which in this case is merely an elastic layer, since it is not actuated) by even a negligibly small length leads to increase in bending deflection by about 3.9%. However, the deflection remains unchanged, irrespective of further increase in debonded length of extension actuator by any extent as shown in Fig. 9(c). Because, the stiffness right at the fixed end plays a crucial role for a beam with full length actuators under SAM. That is, even a peel-off at the fixed end renders the rest of the extension actuator almost dysfunctional regarding its contribution to the stiffness. The clamped-free beam under HAM also undergoes decreasing deflection with increase in the length of debonding of extension actuator (Fig. 9(d)). However, the percentage reduction in deflection for a given length of debonded extension actuator is slightly less than that in case of EAM. This behavior is attributed to the response of the beam under SAM component of HAM as explained already.

Hinged-hinged beam under EAM does not show appreciable decrease in the deflection up to about 10% edge debonding (Fig. 9(e)), since negligibly small reduction in stiffness and actuation authority close to hinge support does not affect the deflection much. Further increase in the length of the edge debonding leads to considerable decrease in the deflection. Also, the asymmetry introduced by the edge debonding of extension actuator shifts the location of maximum deflection slightly towards the right side of the mid-point. Hinged-hinged beam under SAM does not undergo deflection (Fig. 9(f)). This is because the beam with full length shear actuator needs atleast one of its ends to be clamped for it to undergo deflection under SAM. However, the beam undergoes

negligibly small deflection due to edge debonding of extension actuator and which remains the same irrespective of the change in the length of edge debonding. This behavior is similar to that of clamped-free beam under SAM. For different extents of edge debonding, the hinged-hinged beam under HAM results in the deflection distribution (Fig. 9(g)), which is exactly similar to that of the beam under EAM (Fig.9(e)), since the deflection of the debonded beam due to SAM component of HAM is negligibly small. Clamped-clamped beam under EAM is simply subjected to block force without any deflection (Raja *et al*. 2004). Nevertheless, the increasing actuator edge debonding makes the beam to undergo deflection, until it attains a sine wave shaped deflection at 50% debonding as shown in Fig. 9(h). The clamped-clamped healthy beam under SAM undergoes a sine wave deflection and this deflection almost remains unchanged with increase in the extent of edge debonding as shown in Fig. 9(i). Under HAM, the clamped-clamped healthy beam undergoes sine wave shaped defection as shown in Fig. 9(j). This is entirely due to the SAM component and as stated already, the clamped-clamped beam under EAM does not undergo deflection. The edge debonding of extension actuator leads to change in the deflection, while the sine wave shape of deflection remains unaffected. Beam with unsymmetrical boundary condition such as hinged-clamped, when subjected to EAM does not show appreciable change in deflection till about 10% of actuator debonding on the hinge support side (Fig. 9(k)). Because, the reduction in bending stiffness and actuation authority at a region close to the hinge support does not affect the deflection much. Further increase in debonding, however, results in considerable reduction in the deflection. After about 30% debonding onwards, deviation in the deflection curve can be witnessed. When debonding is considered at the clamped end of the clamped-hinged beam under EAM (Fig. 9(l)), the deflection increases till about 20% of debonding. Here, reduction in bending stiffness at the clamped end has larger influence on the electro-mechanical stiffness. Further increase in debonding leads to reduction in deflection, indicating that loss in effective length of actuator now plays major role in reducing the electromechanical stiffness.

Bending deflection behaviour of the beam with different extents and location of inner debonded extension actuator is investigated. It is found that the inner debonding of extension actuator to any extent and under EAM does not influence the actuation authority of the beam. As the extension actuator is known to produce boundary forces, the actuation authority of debonded portion of extension actuator is not degraded until it buckles (Ikeda *et al*. 2010). Furthermore, as already discussed, the deflection of the beam under SAM is not affected due to negligibly small reduction in the stiffness of the beam.

8.2 Debonding of top face

Both elastic layer and piezoelectric layer in the top face together are debonded from the top surface of the core leading to significant drop in the bending stiffness of the beam. To visualize the extent of loss in the bending stiffness, the clamped-free sandwich beam is subjected to a point force of 100 N at the free end and the deflection distributions for different percentages of edge debonding of the top face at the clamped end are plotted as shown in Fig. 10(a). Substantial loss in the bending stiffness is evident from the increase in the free end deflection with the increase in the percentage of edge debonding. For instance, the increase in deflection with increase in the edge debonding by 30% is 34.9% with respect to the deflection of the healthy beam. Clamped-free beam under EAM undergoes increasing deflections with increase in the percentage of edge debonding of top face as can be seen from Fig. 10(b). The reduction in the effective length of the top extension actuator due to debonding of top face should result in decreasing deflection. On the

contrary, the tendency of increasing deflections indicates that the loss of bending stiffness dominates over the loss of the actuation authority. Shear actuated (SAM) clamped-free beam with 10% of edge debonded top face at the fixed end undergoes deflection, which is 38% of that of the healthy beam as shown in Fig. 10(c). Further increase in the top face debonding by any length does not cause any change in deflection. The shear actuation needs sandwich beam construction in which the shear actuator in the core is sandwiched between the elastic layers. However, just the separation of top face from the clamped end is analogous to having the shear actuator with only the bottom face. That is, the debonded top face merely behaves as a rigid body attached to the top surface of the shear actuator not contributing to the stiffness. This is indicative of the enormity of damage done to the beam. The clamped-free beam under HAM, with increase in edge debonding of top face also causes increase in deflection (Fig. 10(d)). However, the percentage of increase in the deflection is less than that of EAM. Decrease in the deflection due to the SAM component of HAM is responsible for this behaviour. Hinged-hinged beam with edge debonding on one of the ends, when subjected to EAM undergoes increase in deflection until about 30% debonding due to reduction in bending stiffness (Fig. 10(e)). However, with further increase in debonding, there is only slight decrease in deflection. This behaviour is attributed to the debonding of actuator (leading to the loss of actuation performance) along with the elastic layer. A full-length shear actuator in the sandwich needs at least one clamped end of the beam for the actuation. Therefore, hinged-hinged beam does not undergo any deflection under the influence of SAM. However, the damage caused by the increasing length of the debonded top face results in increasing deflection (Fig. 10(f)). When subjected to HAM, the hinged-hinged beam undergoes deflections, which are algebraic summations of deflections due to EAM and SAM components. Observe that the deflection under HAM, with 10% edge debonding is less than that under EAM (Fig. 10(g)), since the deflection due to SAM component and with the same percentage of debonding is negative for most of the length of the beam. As already pointed out, clamped-clamped beam under the influence of EAM does not undergo any deflection. However, increasing top face debonding makes the beam to undergo deflection that changes from positive side to negative side (Fig. 10(h)). Clamped-clamped beam under SAM is subjected to sine wave shaped deflection until about 20% edge debonding (Fig. 10(i)). But, further increase in the edge debonding results in deflection distribution curve, which is no more a sine wave shaped curve. Healthy clamped-clamped beam under HAM undergoes sine wave shaped deflection. This deflection is due to SAM component of HAM, while the EAM component not causing any deflection to be induced is redundant. But the debonding of face results in deflection, which is no more a sine wave shaped curve, as shown in Fig. 10(j). The sandwich beam with the unsymmetrical boundary conditions such as hinged-clamped and under the influence of EAM, behaves almost similar to the case of top actuator debonding but with different deflections (Fig. 10(k)). When the edge debonding is at the clamped end, the deflections due to different percentages of debonding are much larger than those with the debonding at the hinged end as shown in Fig 10(l). The edge debonding at the clamped end leads to substantial loss in the bending stiffness of the beam.

The inner debonding of top face does not affect the deflection due to EAM or SAM much. The inner deboneded region has top and bottom regions separated by the plane of debonding and these regions are between the two healthy regions as shown in Fig. 3. The top and bottom debonded regions with their axes offset from the axis of the healthy region are subjected to extension and compression, leading to differential stretching (Mujumdar and Suryanarayan 1988). This phenomenon is due to continuity of displacements between the debonded and healthy regions. The

loss in bending stiffness due to debonding is compensated by the additional stiffness induced by the differential stretching.
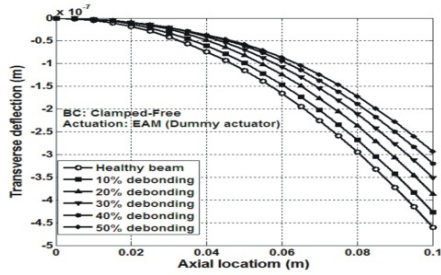

(a) Clamped-free EAM (Dummy actuator)
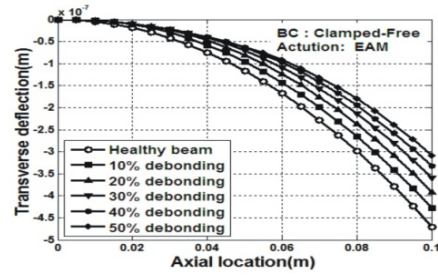
(b) Clamped-free EAM
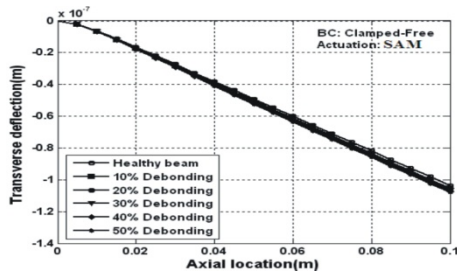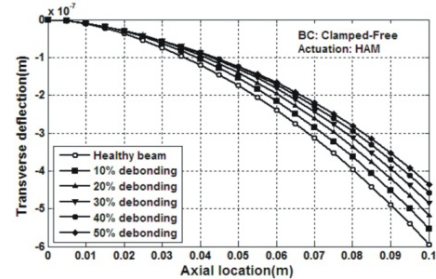
(c) Clamped-free SAM

(d) Clamped-free HAM
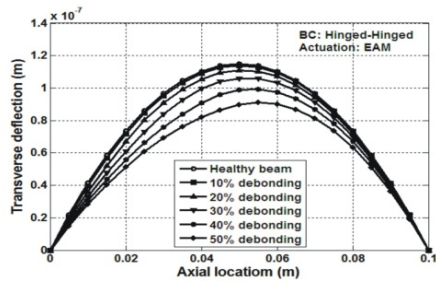
(e) Hinged-hinged EAM
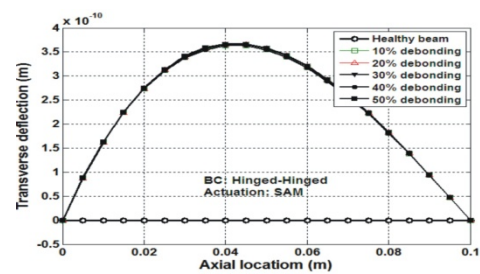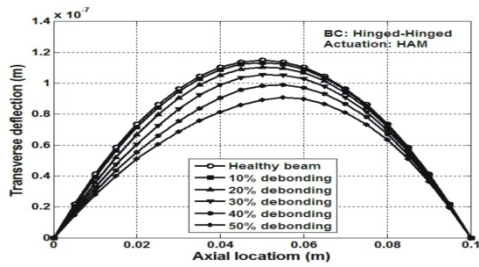
(f) Hinged-hinged SAM
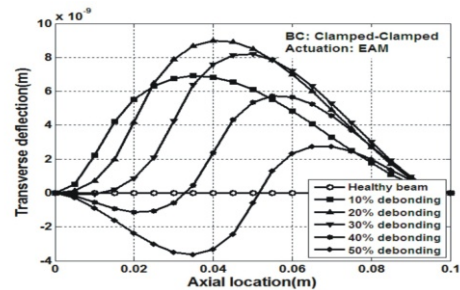
(g) Hinged-hinged HAM

(h) Clamped-clamped EAM

Continued-
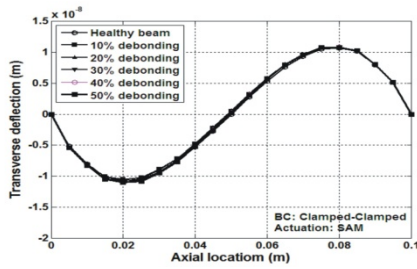
(i) Clamped-clamped   SAM
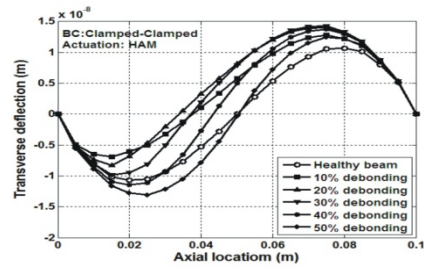
(j) Clamped-clamped HAM
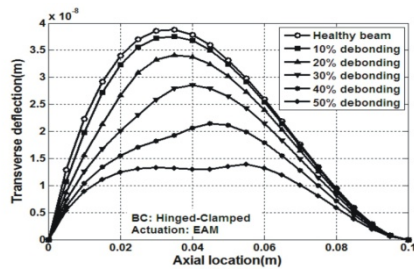

(k) Hinged-clamped   EAM
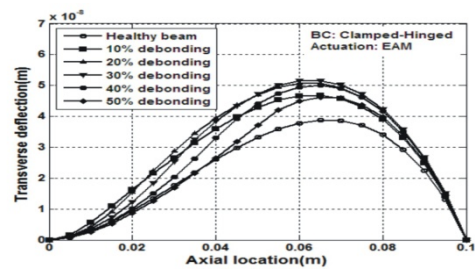
(l) Clamped-hinged EAM

Fig. 9 Deflection distributions of sandwich beam with debonded top extension actuator
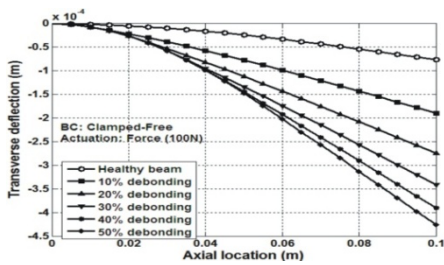
(a) Clamped-free Force
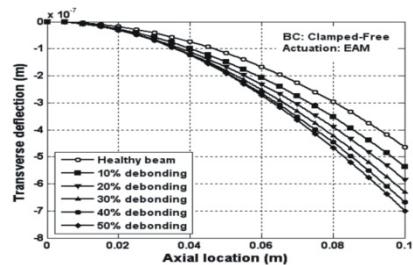
(b) Clamped-free EAM
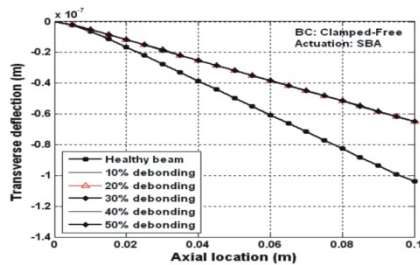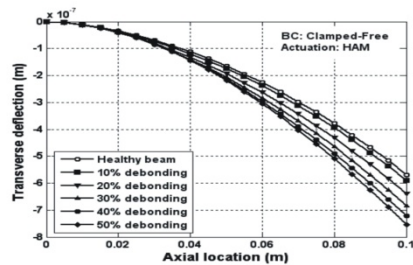
(c) Clamped-free   SAM

(d) Clamped-free HAM

Continued-
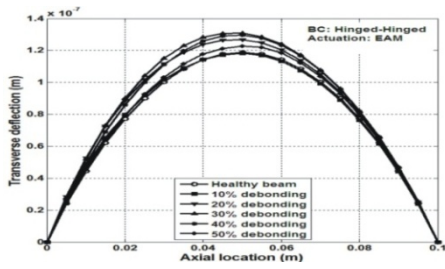
(e) Hinged-hinged   EAM
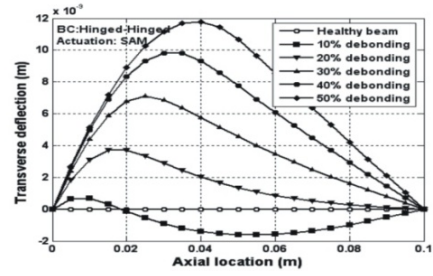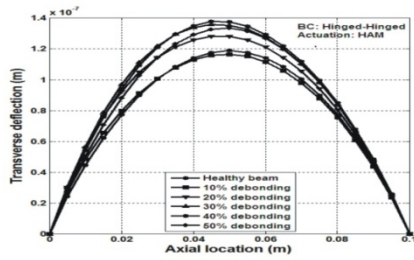
(f) Hinged-hinged SAM
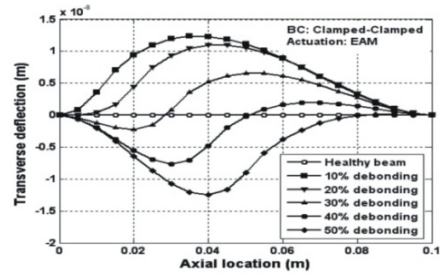
(g) Hinged-hinged   HAM

(h) Clamped-clamped EAM
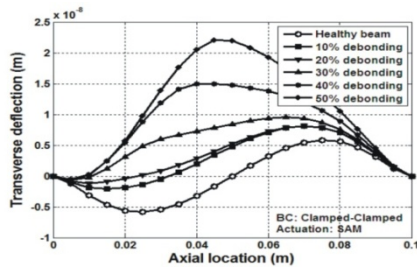
(i) Clamped-clamped SAM
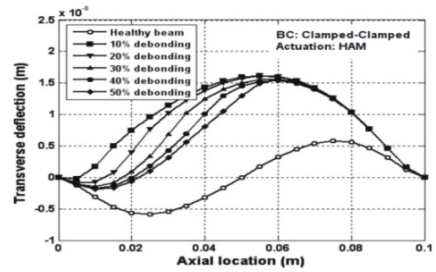
(j) Clamped-clamped HAM
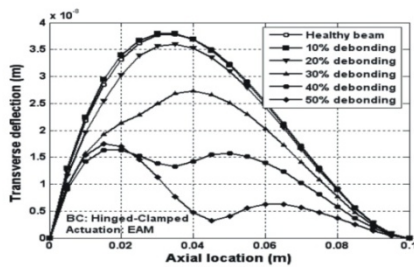
(k) Hinged-clamped EAM
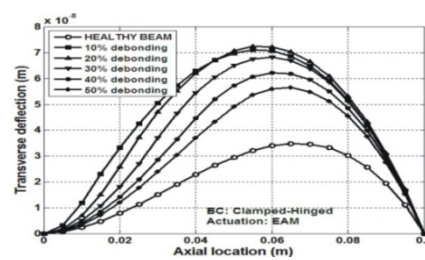
(k) Clamped-hinged EAM

Fig. 10 Deflection distributions of adaptive sandwich beam with debonded top face

9. Conclusions

The formulated two noded coupled beam element is adopted for modeling healthy sandwich beam and beam with extension actuator/face debonding, with different boundary conditions and actuation types. Investigations on the bending behaviour are carried out by conducting several numerical experiments. The numerically estimated deflection distributions of the sandwich beam with the edge debonding of extension actuator and under EAM are validated with the experimental values.   Different parameters considered for this study are, extension actuator/face debonding, type of debonding (edge/inner debonding), length of debonding, actuation type (EAM, SAM or HAM) and different boundary conditions. Important findings are presented below.

1. Clamped-free Sandwich beam under EAM undergoes decreasing deflections with the increasing extent of edge debonded extension actuator. Extension actuator debonding results in substantial degradation in the actuation authority, while the bending stiffness is not affected much. Under the influence of SAM, the clamped-free beam is subjected to very small increase in the deflection, which remains constant for any extent of extension actuator debonding.

2. The clamped-free beam under EAM undergoes increasing deflection with increase in the extent of edge debonding of face. This is due to significant loss in the bending stiffness. Therefore, in case of edge debonding of face, reduction in bending stiffness has large influence on electromechanical stiffness than the reduction in actuation authority has. There is large decrease in the deflection of clamped-free beam under SAM, for even a very small length of edge debonding of face. The deflection remains the same irrespective of further increase in the edge debonding.

3. Deflection distributions of hinged-hinged sandwich beam under EAM, with different extents of debonding of extension actuator are exactly same as those of the beam under HAM. The reason for this is attributed to negligibly small deflections of the hinged-hinged beam under SAM, with different extents of debonding. However, the situation is different with the edge debonding of face, where the deflections due to HAM, in general, for different extents of debonding are slightly larger than those under the influence of EAM.

4. Clamped-clamped beam with 10% edge debonded extension actuator and under EAM undergoes a positive deflection, which gradually changes to a sine wave shaped deflection with edge debonding of extension actuator by 50%. Whereas, the edge debonding of face under similar conditions results in the positive deflection distribution at 10% debonding, which changes gradually to negative deflection distribution at 50% edge debonding. Under SAM, the clamped-clamped beam with increasing extension actuator debonding undergoes negligibly small deflections. Contrary to this, the increasing extent of face results in considerable increase in the deflection distributions.

5. The inner debonding of extension actuator / face does not affect the actuation authority.

Acknowledgements

References

Baillargeon, B.P. and Vel, S.S. (2005), "Active vibration suppression of sandwich beams using piezoelectric shear actuators: experiments and numerical simulations", *J. Intel. Mater. Syst. Str.*, **16**(6), 517-530.

Benjeddou, A., Trindade, M.A. and Ohayon, R. (1999), "New shear actuated smart structure beam finite element", *AIAA J.*, **37**(3), 378-383.

Ikeda, T., Raja, S. and Ueda, T. (2010), "Deformation of a beam with partially debonded piezoelectric actuators", *J. Intel. Mater. Syst. Str.*, **21**(4), 453-468.

Kapuria, S and Yaqoob Yasin, M, (2010), "Active vibration control of piezoelectric laminated beams with electrode actuators and sensors using an efficient finite element involving an electric node", *Smart Mater. Struct.*, **19**(4), 1-15.

Kapuria, S. and Hagedorn, P. (2007), "Unified efficient layerwise theory for smart beams with segmented extension/shear mode, piezoelectric actuators and sensors", *J. Mech. Mater. Struct.*, **2** (7), 1267-1297.

Kapuria, S., and Alam, N. (2006), "Efficient layerwise finite element model for dynamic analysis of laminated piezoelectric beams", *Comput. Method. Appl. M.*, **195**(19-22), 2742-2760.

Kapuria, S., Kumari, P and Nath, J.K, (2010), "Efficient modeling of smart piezoelectric composite laminate- A review", *Acta Mech.*, **214**(1-2), 31-48.

Khadeir, A.A. and Aldreihm, O.J. (2001), "Deflection analysis of beams with extension and shear piezoelectric patches using discontinuity functions", *Smart Mater. Struct.*, **10** (2), 212-220.

Koconis, D.B., Kollar, K.P. and Springer, G.S. (1994), "Shape control of composite plates and shells with embedded actuators, I- voltages specified", *J. Compos. Mater.*, **28**(3) 415-458.

Kumar, R., Mishra, B. K. and Jain, S.C. (2008), "Static and dynamic analysis of smart cylindrical shell", *Finite Elem. Anal. Des.*, **45**(1), 13-24.

Kusculuoglu, Z.K., Fallahi, B. and Royston, T.J. (2004), "Finite element model of a beam with piezoceramic patch actuator", *J. Sound Vib.*, **276**(1-2), 27-44.

Lee, H.J. (2005), "Layerwise laminate analysis of functionally graded piezoelectric bimorph beams", *J. Intel. Mater. Syst. Str.*, **16**(4), 365-371.

Li, Y.Y., Cheng, L., Yam, L.H. and Yan, Y.J. (2003), "Numerical modeling of a damaged plate with piezoelectric actuation", *Smart Mater. Struct.*, **12**(4), 524-532.

Mujumdar, P.M. and Suryanaryana, S. (1988), "Flexural vibrations of beams with delaminations", *J. Sound Vib.*, **125**(3), 441-461.

Manjunath, T.C. and Bandyopadhyay, B. (2009),"Vibrational control of Timoshenko smart structures using multirate output feedback based discrete sliding mode control for SISO systems", *J. Sound Vib.*, **326** (1-2), 50-74.

Nagendra K.D., Raja, S. and Ikeda, T. (2007), "Active vibration control of smart plates with partially debonded multi-layered PZT actuators", *Smart Mater. Struct.*, **16**(5), 1584-1594.

Raja, S., Prathap, G. and Sinha, P.K. (2002), "Active vibration control of composite sandwich beams with piezoelectric extension-bending and shear actuators", Smart *Mater. Struct.*, **11**(1), 63-71.

Raja, S., Sreedeep, R. and Prathap, G. (2004), "Bending behavior of hybrid-actuated piezoelectric sandwich beams", *J. Intel. Mater. Syst. Str.*, **15** (8) 611-619.

Seeley, C.E. and Chattopadyay, A. (1999), "Modeling of adaptive composites including debonding", *Int. J. Solids Struct.*, **36**(12), 1823 -1843.

Singh, S.K., Chakrabarti, A., Bera, P. and Sony, J.S.D. (2011), "An efficient C[0] FE model for the analysis of composites and sandwich laminates with general layup", *Lat. Am. J. Solids. Struct.*, **8**(2), 197-212.

Sun, D. and Tong, L. (2004), "An equivalent model for smart beams with debonded piezoelectric patches", *J. Sound Vib.*, **276**(3-5), 933-956.

Sun, D., Tong, L. and Satya, N.A. (2001), "Effects of piezoelectric sensor/actuator debonding on vibration control of smart beams", *Int. J. Solids Struct.*, **38**(50-51), 9033-9051.

Wang, S.Y. (2004), "A finite element model for the static and dynamic analysis of piezoelectric bimorph",

Int. J. Solids Struct., **41**(15), 4075-4096.
www.sparklerceramics.com/piezoelectric properties.html, Sparkler Ceramics Pvt Ltd
Zhang, X.D. and Sun, C.T. (1996), "Formulation of an adaptive sandwich beam", *J. Intel. Mater. Syst. Str*., **5**(6), 814-823.

CY

Appendix A: Penalty matrices for displacement continuity conditions

Table A1 Top extension actuator debonding

Healthy region-bottom debonded region:	*Healthy region -top debonded region:*
$P_{ii}^{S1} = \begin{bmatrix} 1 & -r_{12} & 0 & 0 \\ -r_{12} & (r_{12}^2 +1) & 0 & 0 \\ 0 & 0 & 1 & 0 \\ 0 & 0 & 0 & 1 \end{bmatrix}$	$P_{ii}^{S2} = \begin{bmatrix} 1 & (r_{13} -z_t) & 0 & -z_t \\ (r_{13} -z_t) & (r_{13} -z_t)^2 & 0 & -z_t(r_{13} -z_t) \\ 0 & 0 & 1 & 0 \\ -z_t & -z_t(r_{13} -z_t) & 0 & (z_t^2 +1) \end{bmatrix}$
$P_{ij}^{S1} = \begin{bmatrix} -1 & 0 & 0 & 0 \\ r_{12} & -1 & 0 & 0 \\ 0 & 0 & -1 & 0 \\ 0 & 0 & 0 & -1 \end{bmatrix}$	$P_{ij}^{S2} = \begin{bmatrix} -1 & 0 & 0 \\ -(r_{13} -z_t) & 0 & 0 \\ 0 & -1 & 0 \\ z_t & 0 & -1 \end{bmatrix}$
$P_{jj}^{S1} = \begin{bmatrix} 1 & 0 & 0 & 0 \\ 0 & 1 & 0 & 0 \\ 0 & 0 & 1 & 0 \\ 0 & 0 & 0 & 1 \end{bmatrix}$	$P_{jj}^{S2} = \begin{bmatrix} 1 & 0 & 0 \\ 0 & 1 & 0 \\ 0 & 0 & 1 \end{bmatrix}$

Table A2: Top face debonding

Healthy region-bottom debonded region	*Healthy region-top debonded region*
$P_{ii}^{S1} = \begin{bmatrix} 1 & -(r_{12} +z_t) & 0 & -z_t \\ -(r_{12} +z_t) & (r_{12} +z_t)^2 +1 & 0 & z_t(r_{12} +z_t) \\ 0 & 0 & 1 & 0 \\ -z_t & z_t(r_{12} +z_t) & 0 & z_t^2 +1 \end{bmatrix}$	$P_{ii}^{S2} = \begin{bmatrix} 1 & r_{13} & 0 & 0 \\ r_{13} & r_{13}^2 & 0 & 0 \\ 0 & 0 & 1 & 0 \\ 0 & 0 & 0 & 1 \end{bmatrix}$
$P_{ij}^{S1} = \begin{bmatrix} -1 & 0 & 0 & 0 \\ (r_{12} +z_t) & -1 & 0 & 0 \\ 0 & 0 & -1 & 0 \\ z_t & 0 & 0 & -1 \end{bmatrix}$	$P_{ij}^{S2} = \begin{bmatrix} -1 & 0 & 0 \\ -r_{13} & 0 & 0 \\ 0 & -1 & 0 \\ 0 & 0 & -1 \end{bmatrix}$
$P_{jj}^{S1} = \begin{bmatrix} 1 & 0 & 0 & 0 \\ 0 & 1 & 0 & 0 \\ 0 & 0 & 1 & 0 \\ 0 & 0 & 0 & 1 \end{bmatrix}$	$P_{jj}^{S2} = \begin{bmatrix} 1 & 0 & 0 \\ 0 & 1 & 0 \\ 0 & 0 & 1 \end{bmatrix}$